ISSN 1392 - 1207. MECHANIKA. 2013 Volume 19(3): 277-282

RANS simulations of turbulent and thermal mixing in a T-junction

M. Aounallah*, M. Belkadi, L. Adjlout***,O. Imine******

**Laboratoire d'Aéro-Hydrodynamique Navale, USTOran MB, Algeria, E-mail:aounallah_2000@yahoo.fr*
***Laboratoire d'Aéro-Hydrodynamique Navale, USTOran MB, Algeria, E-mail:belkadigma@yahoo.fr*
****Laboratoire d'Aéro-Hydrodynamique Navale, USTOran MB, Algeria, E-mail:adjloutl@yahoo.fr*
*****Laboratoire d'Aéronautique et Systèmes Propulsifs, USTOran MB, Algeria, E-mail: imine_omar@yahoo.fr*

crossref http://dx.doi.org/10.5755/j01.mech.19.3.4663

1. Introduction

The large temperature fluctuations of the fluid can causes a serious disturbance in the operating conditions of some machines which require uniform temperature field at its inlets. For this reason, engineers in many industrial applications try to determine the shortest length of the pipelines to avoid this problem. Moreover, in the place where cold and hot fluids are mixed, a high cycle thermal fatigue in surrounding structure occurs. This phenomenon is significant for structural integrity and safety of the plant. Throughout the world, many reactors were shut down due to the leakage in light water circuit such as the Japanese PWR Tomari-2 in 2003 and the French PWR Civaux in 1998.

Recently some experiments have produced reliable data for validation of computational fluid dynamics (CFD) calculations. Westin et al. [1-2] describes new experimental data of thermal mixing in a T-junction to be used for comparisons. The authors have found that the LES and DES results were in qualitative good agreement with the new experimental data published also when fairly coarse computational meshes were used. Walker et al. [3] have carried out a T-junction mixing experiment with wire-mesh sensors and they obtain important information on the scale of turbulent mixing patterns by cross-correlating the fluctuations signal recorded at different locations within the measuring plane of the sensor. Kimura et al. [4] have studied the influence of upstream elbow in the main pipe of a mixing tee facility. Measured temperature showed that fluctuation intensity near the wall was larger in the case with elbow than in the straight case under the wall jet condition. Naik-Nimbalkar et al. [5] have carried out experiments and numerical investigations of thermal mixing in a T-junction with water. The numerical predictions of the velocity and the temperature fields are found in good agreement with the experimental data.

In the last decades, the flow in T-junctions becomes a challenging test case for CFD. The majority of the numerical contributions underline a number of difficulties principally related to turbulence modeling and the coupling between the turbulence and the heat flux. Walker et al. [6] have performed steady-state calculations with ANSYS-CFX-10 using the *k-ε*, *k-ω SST* and *RSM* models. It was found that both turbulent mixing and turbulent momentum transport downstream of the side-branch connection are underestimated by all the three models and the calculated transport scalar and velocity profiles are less uniform than the measured ones. Better results were obtained by increasing of the model coefficient C_μ in the *k-ε* model leading to an improvement of velocity profiles. Frank et al. [7] have simulated the turbulent isothermal and thermal mixing phenomena using ANSYS CFX 11.0 with unsteady Reynolds averaging *SST* and *RSM* and with scale-resolving *SAS-SST* turbulence models. It has demonstrated that unsteady *SST* or *RSM* turbulence models are able to satisfactorily predict the turbulent mixing of isothermal water streams in a T-junction in the horizontal plane and transient thermal striping was observable from the *SAS-SST* solution. Chapuliot et al. [8] have inspected the incident of the residual heat removal system of the Civaux unit 1 reactor. Sinkunas et al [9] have used a method for the calculations of heat transfer and friction in laminar film with respect to variability of liquid physical properties. The dependencies of stabilized heat transfer and friction on temperature gradient for laminar film flow were estimated analytically. Using the CAST3D code, the thermo-hydro-mechanical simulation has demonstrated that the critical point of the accident was the appearance of a crack on the outside of the bend and its rapid propagation through the wall.

Passuto et al. [10] have simulated the turbulent flow using LES technique with Code_Saturne developed by EDF in order to follow the influence of the mean and fluctuating quantities when upstream elbows are neglected in a T-junction. Many others works relating to the thermal mixing using LES were documented in the literature; see e.g. Kuczaj et al. [11], Lu et al. [12].

To gain some understanding of the phenomena taking place in the mixing zone in T-junctions, numerical investigations have been carried out to determine the thermal mixing length. The simulations were done using steady 3D approach and the turbulent fluid motion was solved with RANS: *k-ε* standard, *k-ω* standard, *k-ω SST* and *RSM* models. The tests were conducted to predict the flow field and the temperature distribution inside a horizontally oriented T-junction with a straight main pipe and a side branch coming in under an angle of 90°.

2. Problem position

The problem treated is basically a three dimensional turbulent thermal flow inside T-pipes with an angle of 90°. Fig. 1 shows the geometrical features of the horizontally oriented T-junction under consideration and the coordinates chosen. The simulation domain consists of the main pipe with a length of 80 inch and a diameter of 6 inch and the side branch which is 30 inch long and 2 inch diameter. The junction is positioned at 1/4 of length of the main pipe.Cold water flows from the left of the main pipe at

15°C and the hot water incomes from the small branch at 50°C. The temperature difference is set to 35°C. The approximate cold and hot flow rates are 30 and 20 m^3/h giving inlet bulk velocity values of 0.45–2.74 m/s and the corresponding Reynolds numbers are (0.7–1.37) × 10^5 respectively. During the simulations, it is assumed that there is no heat exchange with the exterior and all the thermophysical proprieties of water (viscosity, diffusivity and the specific heat at constant pressure) are set constant except density is function of temperature.

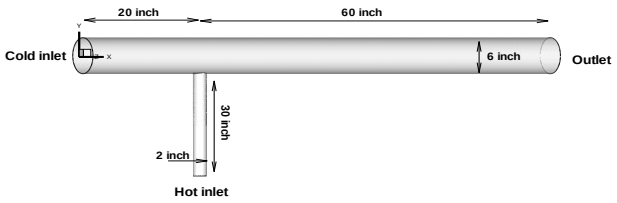

Fig. 1 Geometry and boundary conditions for the T-junction

3. Grid generation

Fig. 2 shows the junction zone of the computational domain meshed with hexahedral control volumes. The geometry and the mesh are generated using Gambit preprocessor taking into account the boundary layer refinement with 6 layers near both pipes walls. The height of the first cell is calculated through the estimation of the y+ value which guarantees the use of the high Reynolds number turbulence models with an acceptable accuracy. The mesh quality is excellent since 71% of total cells have an equisize skew coefficient less than 0.1 and 19% between 0.1 and 0.2. The remaining cellules have this coefficient between 0.2 and 0.4. Several tests of grid sensitivity were carried out to get independent solution and finally a grid resolution of 575 280 hexahedral cellules is employed.

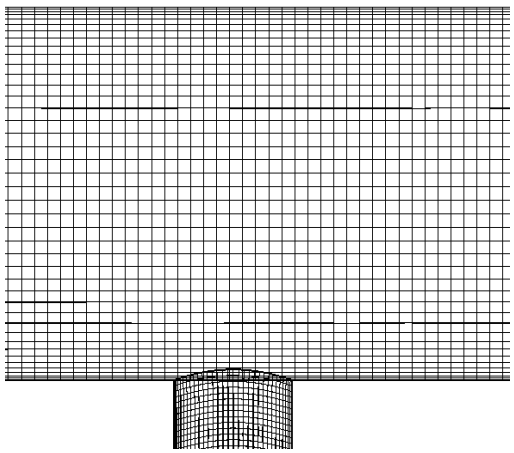

Fig. 2 Hexahedral mesh generated for the T-junction

4. Mathematical formulation

The problem treated is a steady three-dimensional flow in a main pipe with an incoming branch of 90°. The Reynolds number based on the velocity at the centreline and the diameter of the cold inlet is set to 0.7 10^5. The non-isothermal viscous incompressible flow inside the pipes is described by the steady-state Navier-Stokes equations and the conservation of energy balance. The governing equations are defined as follows

$$\frac{\partial}{\partial x_j}\left(\rho u_j\right) = 0 \tag{1}$$

$$\frac{\partial}{\partial x_j}\left(\rho u_j u_i\right) = -\frac{\partial P}{\partial x_i} + \frac{\partial}{\partial x_j}\left[\left(\mu + \mu_t\right)\left(\frac{\partial u_i}{\partial x_j} + \frac{\partial u_j}{\partial x_i}\right)\right] -$$

$$-\frac{2}{3}\frac{\partial}{\partial x_j}\left(\mu_t \frac{\partial u_j}{\partial x_j}\right), \qquad i = 1,2,3 \tag{2}$$

$$\frac{\partial}{\partial x_j}\left(\rho u_j T\right) = \frac{\partial}{\partial x_j}\left[\left(\frac{\lambda}{C_p} + \frac{\mu_t}{\sigma}\right)\frac{\partial T}{\partial x_j}\right] \tag{3}$$

The density is calculated by Eq. (4) in which the temperature is taken in Kelvin unit.

$$\rho = -0.00407\, T^2 + 2.1697\, T + 711.66 \tag{4}$$

The turbulent viscosity is modelled by four turbulence models: the standard *k-ε* model of Launder [13], the *k-ω* Standard of Wilcox [14] and the *k-ω SST* of Menter [15]. The *RSM* model of Launder [16] closes the RANS equations by solving seven Reynolds stresses transport equations, together with an equation for the dissipation rate. For a simple presentation, only the overall forms of equations are given.

4.1. *k-ε* Standard model

$$\frac{\partial}{\partial x_j}\left(\rho k u_j\right) = \frac{\partial}{\partial x_j}\left[\left(\mu + \frac{\mu_t}{\sigma_k}\right)\frac{\partial k}{\partial x_j}\right] + G_k - \rho\varepsilon \tag{5}$$

$$\frac{\partial}{\partial x_j}\left(\rho \varepsilon u_j\right) = \frac{\partial}{\partial x_j}\left[\left(\mu + \frac{\mu_t}{\sigma_\varepsilon}\right)\frac{\partial \varepsilon}{\partial x_j}\right] +$$

$$+C_{1\varepsilon}\frac{\varepsilon}{k}G_k - C_{2\varepsilon}\,\rho\frac{\varepsilon^2}{k} \tag{6}$$

$$\mu_t = \rho C_\mu \frac{k^2}{\varepsilon} \tag{7}$$

G_k represents the production of turbulence kinetic energy due to the mean velocity gradients and the constants are: $C_{1\varepsilon} = 1.44$, $C_{2\varepsilon} = 1.92$, $C_\mu = 0.09$, $\sigma_k = 1.0$, $\sigma_\varepsilon = 1.3$.

4.2. *k-ω* Standard model

$$\frac{\partial}{\partial x_j}\left(\rho k u_j\right) = \frac{\partial}{\partial x_j}\left[\left(\mu + \frac{\mu_t}{\sigma_k}\right)\frac{\partial k}{\partial x_j}\right] + G_k - Y_k \tag{8}$$

$$\frac{\partial}{\partial x_j}\left(\rho \omega u_j\right) = \frac{\partial}{\partial x_j}\left[\left(\mu + \frac{\mu_t}{\sigma_\omega}\right)\frac{\partial \omega}{\partial x_j}\right] + G_\omega - Y_\omega \tag{9}$$

$$\mu_t = \alpha^* \frac{\rho k}{\omega} \tag{10}$$

G_k represents the generation of turbulence kinetic energy, G_ω represents the generation of specific dissipartion rate. Y_k and Y_ω represent the dissipation of *k*

and ω due to turbulence. The coefficient α^* damps the turbulent viscosity causing a low-Reynolds-number correction. The constants are: $\sigma_k = 2.0$ and $\sigma_\omega = 2.0$.

4.3. *k-ω SST* model

$$\frac{\partial}{\partial x_j}\left(\rho k u_j\right) = \frac{\partial}{\partial x_j}\left[\left(\mu + \frac{\mu_t}{\sigma_k}\right)\frac{\partial k}{\partial x_j}\right] + \tilde{G}_k - Y_k \quad (11)$$

$$\frac{\partial}{\partial x_j}\left(\rho \omega u_j\right) = \frac{\partial}{\partial x_j}\left[\left(\mu + \frac{\mu_t}{\sigma_\omega}\right)\frac{\partial \omega}{\partial x_j}\right] + \\ + G_\omega - Y_\omega + D_\omega \quad (12)$$

$$\mu_t = \frac{\rho k}{\omega}\frac{1}{max\left[\frac{1}{\alpha^*}, \frac{S F_2}{a_1 \omega}\right]} \quad (13)$$

$\tilde{G}_k$ represents the generation of turbulence kinetic energy, G_ω represents the generation of specific dissipartion rate. Y_k and Y_ω represent the dissipation of k and ω due to turbulence. D_ω represents the cross-diffusion term. The coefficient α^* damps the turbulent viscosity causing a low-Reynolds-number correction. S is the strain rate magnitude. F_2 is a blending coefficient. The constants σ_k and σ_ω are the turbulent Prandtl numbers and $a_1 = 0.31$.

4.4. *RSM* model

$$\frac{\partial}{\partial x_k}\left(\rho u_k \overline{u_i' u_j'}\right) = -\frac{\partial}{\partial x_k}\left[\rho \overline{u_i' u_j' u_k'} + \overline{p\left(\delta_{kj} u_i' + \delta_{ik} u_j'\right)}\right] + \\ + D_{L,ii} + P_{ij} + \varphi_{ij} - \varepsilon_{ij} \quad (14)$$

$$\frac{\partial}{\partial x_j}\left(\rho k u_j\right) = \frac{\partial}{\partial x_j}\left[\left(\mu + \frac{\mu_t}{\sigma_k}\right)\frac{\partial k}{\partial x_j}\right] + \frac{1}{2}P_{ii} - \rho\varepsilon \quad (15)$$

$$\frac{\partial}{\partial x_j}\left(\rho \varepsilon u_j\right) = \frac{\partial}{\partial x_j}\left[\left(\mu + \frac{\mu_t}{\sigma_\varepsilon}\right)\frac{\partial \varepsilon}{\partial x_j}\right] + \\ + C_{1\varepsilon}\frac{1}{2}P_{ii}\frac{\varepsilon}{k} - C_{2\varepsilon}\rho\frac{\varepsilon^2}{k} \quad (16)$$

$$\mu_t = \rho C_\mu \frac{k^2}{\varepsilon} \quad (17)$$

$D_{L,ij}$,P_{ij} do not require any modeling, they represent the molecular diffusion and the stress production respectively. However, Φ_{ij} and ε_{ij} represent the pressure strain and the dissipation and need to be modeled to close the Reynolds stress equations. The constants are defined as: $C_{1\varepsilon} = 1.0$, $C_{2\varepsilon} = 1.92$, $C_\mu = 0.09$, $\sigma_k = 0.82$, $\sigma_\varepsilon = 1.0$.

5. Numerical procedure

The conservation Eqs. (1)-(3) coupled with the turbulence transport equations are solved numerically using ANSYS FLUENT 6.3.26 code with the SIMPLE algorithm for coupling pressure-velocity. The momentum, energy and turbulence transport equations are discretized with the second order upwind. Simulations are performed on 4 parallel Intel Xeon 3.2 GHz processors and the steady-state solution is reached after satisfying the convergence criterion based on the maximum residuals of 10^{-6}. In order to obtain a fully developed flow at the hot and cold inlets, a separate computation is firstly conduced on a small cylinder with periodic conditions for both tubes and for the four models of turbulence. The results are obtained after 25 seconds of a transient computation mode; this time seems to be sufficient to achieve a fully developed flow since there is no considerable change in the profile shapes of the velocity components, the turbulent kinetic energy and its dissipation rate. Fig. 3 compares the dimensionless velocity profiles applied at the cold and hot boundary inlets. For both inflows, the velocity profiles intended by the turbulence models experienced collapse approximately in one curve. The velocity, turbulent kinetic energy its dissipation rate planes are saved to be read as boundary conditions at the inlets for the T-junction simulations.

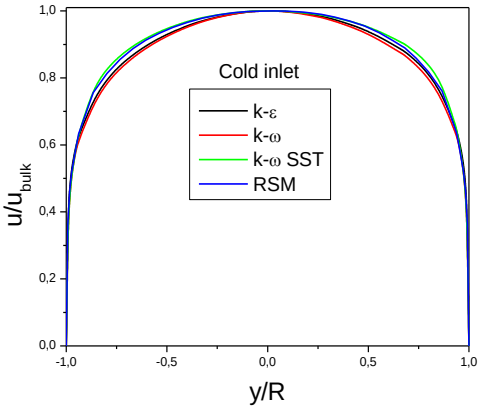

a

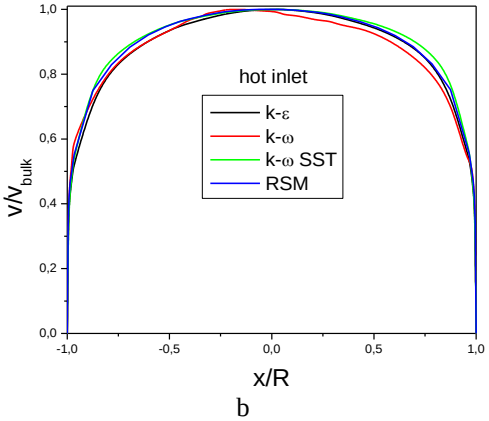

b

Fig. 3 Velocity profiles applied as the boundaryconditions a - cold inlet, b - hot inlet

6. Results

6.1. Convergence

Table compares some convergence characteristics of the simulations conducted for the different turbulence models tested. Numerically, it is clearly seen that each model requires its own iteration number needed to reach convergence. It is also remarked that the CPU time is proportional to the iteration number except for the *RSM* model which requires more CPU time with an iteration number less than that needed by the *k-ω* Standard. It is due certainly to the large number of equations to be solved with the *RSM* compared to those of the two transport equations

models. The convergence is also well recognized by verifying the net imbalance. A very slight imbalance of mass flow rate is observed; without a doubt it is due to numerical diffusion. The temperature at the outlet is well predicted by all the models tested with a slight difference not exceeding 0.8°C.

Table
Some convergence characteristics comparisons between the different models tested

Models	Iterations number	CPU time	Net imbalance of mass flow rate kg/s	Temperature outlet °C
k-ε	500	1h 20’	$-1.54\ 10^{-7}$	21.13
k-ω	1900	3h 10’	$1.16\ 10^{-8}$	20.90
k-ω SST	860	2h 50’	$-6.20\ 10^{-8}$	20.35
RSM	1500	3h 40’	$-8.88\ 10^{-5}$	21.10

6.2. Temperature distribution

Fig. 4 shows the comparison of the dimensionless temperature distribution in the median plane of z-direction for different turbulence models. The numerical predictions show good qualitative agreement between the turbulence models used. The large mass flow rate of the cold water and the small one of the hot stream have made that the hot water does not inward the upper wall of the main pipe and consequently, there is no thermal effect on the structure close to this region. For all the models tested, the upper wall temperature of the main pipe remains constant and equals to the cold temperature. It is also visibly that most heat transfer occurs just in the lower region close the junction. The green zone near the bottom wall of the mixing part represents a division of hot water contoured by cold one since the branch pipe is centered in the perpendicular plan of the main pipe. The mixing region predicted by both standard k-ε and *RSM* models seems to be small and centered in the core of the tube than that simulated by both *k-ω* models which allocate a more melange area going to the outlet.

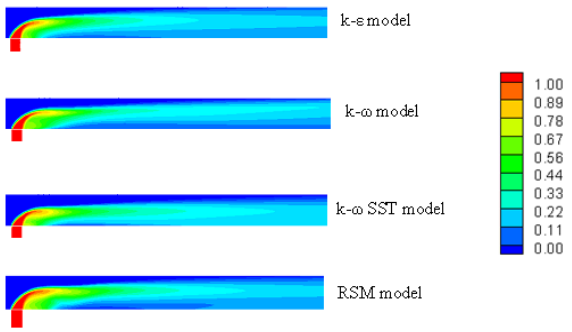

Fig. 4 Dimensionless temperature distribution in the stream-wise direction *z/D* = 0

Fig. 5 indicates a comparison of the dimensionless temperature distribution for several transversal plans vs. turbulence models. To know at what length of the pipe, the flow gets a homogenous temperature, it is more realistic to follow the dimensionless temperature distribution according transversal sections than lines or points probes. So this figure illustrates more truly the thermal mixing phenomenology inside the pipe. For all the simulations carried out, the gradient temperature for different transversal sections decreases with the length of the pipe indicating a gradual thermal mixing between the cold and the hot waters. At the T-junction segment, it is shown that the hot water penetrating in the main pipe is really partial confirming the previous results. The predicted dimensionless temperature distribution at the outlet (*x/L* = 1) by different turbulence models shows diverse sizes of different temperature contours. Nevertheless, this discrepancy does not exceed 0.8°C. In other words, it means that the pipe length is enough to get homogenous temperature if a tolerance of 1°C is considered. Further investigations on a longer pipe can confirm this result and may be getting a uniform temperature distribution without any gradient at its outlet.

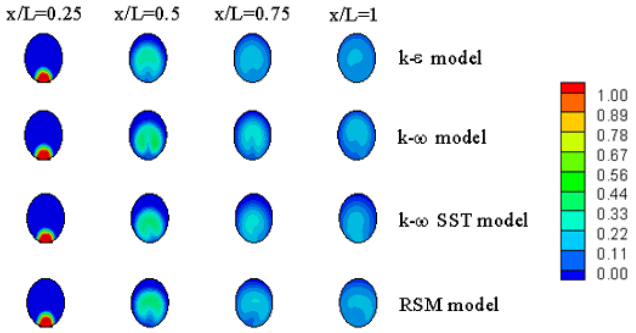

Fig. 5 Cross-sectional distribution of the dimensionless temperature distribution

In Fig. 6, the dimensionless temperature profiles in the y-direction at *x/L* = 0.375 are presented for the various turbulence models. Qualitatively, the same trend is reproduced. The warm water injection upstream this section has increased the fluid temperature from the wall to the center of the pipe. In the remaining region, the dimensionless temperature diminishes quickly and falls to zero due to the important flow mass rate of the cold water compared to the hot one. The pick of the dimensionless temperature is somewhat indistinguishable when both *k-ω* models are used with a slight displacement in the y-direction, while it is underestimated with the *k-ε* model and overestimated with the *RSM* model.

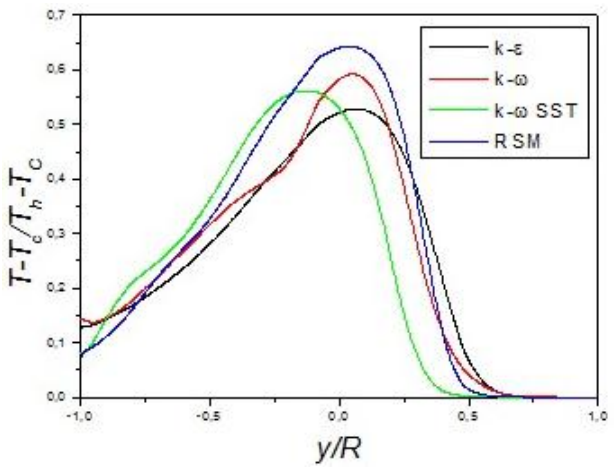

Fig. 6 Dimensionless temperature profiles at *x/L* = 0.375

6.3. Velocity distribution

The dimensionless velocity component in the x-direction profile plotted in the y-direction at $x/L = 0.375$ is shown in Fig. 7. In overall, the numerical predictions obtained by the various turbulence models attest a good qualitative agreement for the two transport equations models while the flow seems to be much accelerated with the *RSM* model. For all the turbulence models, it can be aware that the flow goes faster in the upper rayon than one in the power part. This behavior can be also confirmed by the inequality of the diameter and the flow mass rate of the two pipes.

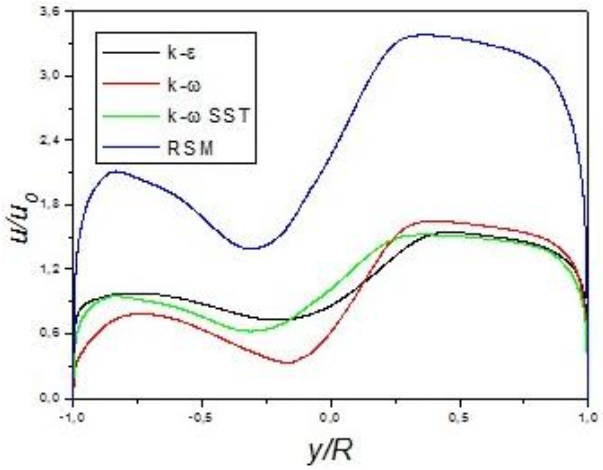

Fig. 7 Dimensionless velocity component profile at $x/L = 0.375$

6.4. Turbulent kinetic energy

Fig. 8 shows the dimensionless kinetic energy in the median plane of z-direction for the different turbulence models. It can be noticed that the high level of turbulence occurs always where the thermal mixing takes place. The area where the maximum turbulent kinetic energy is located with the standard *k-ε* and the *RSM* models is so large compared with that visualized by both *k-ω* models. The dimensionless turbulent kinetic energy profiles in the y-direction at $x/L = 0.375$ are presented for the different turbulence models in Fig. 9. Good qualitative agreement between models is observed with an overestimation on behalf of the *RSM* model as mentioned previously. The turbulent kinetic energy reaches its maximum in the center, where the thermal mixing is high and decreases in both directions towards the walls.

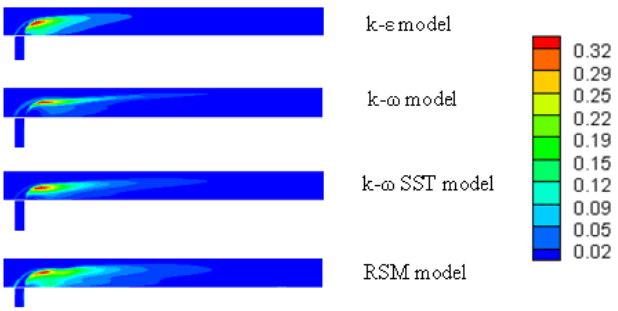

Fig. 8 Dimensionless turbulent kinetic energy distribution in the stream-wise direction $z/D = 0$

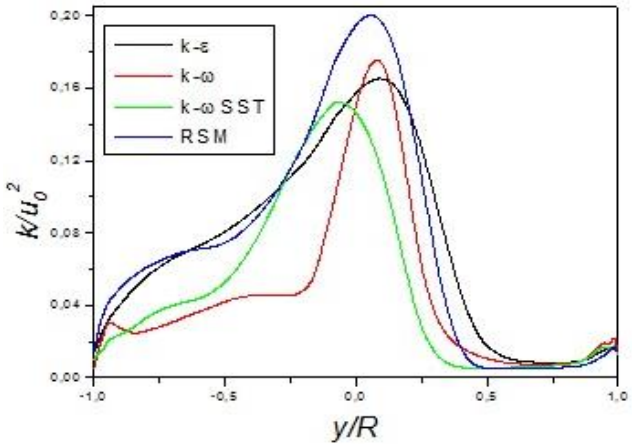

Fig. 9 Dimensionless turbulent kinetic energy profiles at $x/L = 0.375$

7. Conclusion

In the present study, the effect of the RANS turbulence models on the turbulent and thermal fluid mixing is studied. The flow examined is a non-isothermal steady 3D flow in a turbulent regime ($Re = 0.7 \times 10^5$). The aim of this paper is to determine the mixing length where homogenous temperature distribution is established. Exhaustive comparisons have been presented for different flow and temperature parameters function of the different turbulence models.

In general, the results obtained agree qualitatively. Unfortunately, the standard *k-ε* and the *RSM* models predict the flow field and the temperature distribution with some discrepancies, whereas both *k-ω* models are reasonably close between them. It has been numerically demonstrated that the mixing length, at which constant temperature distribution occurs, is at its end ($x/L = 1$) if a tolerance of 1°C is considered. Further simulations on a longer pipe are strongly encouraged to assist in elucidating the length mixing determination.

References

1. **Westin, J.; Alavyoon, F.; Andersson, L.; Veber, V.** 2006. Experiments and unsteady CFD-calculations of the thermal mixing in a T-junction; Workshop on benchmarking of CFD codes for application to nuclear reactor safety (CFD4NRS), IAEA & GRS Garching, Munich., 494-508.
2. **Westin, J.; Veber, P.; Andersson, L.; Mannetje, C.; Andersson, U.; Eriksson, J.; Hendriksson, M.; Alavyoon, F.; Andersson, C.** 2008. High-cycle thermal fatigue in mixing tees. Large-eddy simulations compared to a new validation experiment, 16th Int. Conf. On Nuclear Engineering (ICONE-16), Florida, Orlando, USA, Paper No. 48731:1-11.
3. **Walker, C.; Simiano, M.; Zboray, R.; Prasser, H.-M.** 2009. Investigations on mixing phenomena in single-phase flow in a T-Junction geometry, Nuclear Engineering and Design 239: 116-126. http://dx.doi.org/10.1016/j.nucengdes.2008.09.003.
4. **Kimura, N.; Ogawa, H.; Kamide, H.** 2010. Experimental study on fluid mixing phenomena in T-pipe junction with upstream elbow, Nuclear Engineering and Design 240: 3055-3066.

http://dx.doi.org/10.1016/j.nucengdes.2010.05.019.
5. **Naik-Nimbalkar, V.S.; Patwardhan, A.W.; Banerjee, I.; Padmakumar, G.; Vaidyanathan, G.** 2010. Thermal mixing in T-junctions, Chemical Engineering Science 65: 5901-5911. http://dx.doi.org/10.1016/j.ces.2010.08.017.
6. **Walker, C.; Manera, A.; Niceno, B.; Simiano, M.H.; Prasser, M.** 2010. Steady-state RANS-simulations of the mixing in a T-junction, Nuclear Engineering and Design 240: 2107-2115. http://dx.doi.org/10.1016/j.nucengdes.2010.05.056.
7. **Frank, Th.; Lifante, C.; Prasser, H.M.; Menter, F.** 2010. Simulation of turbulent and thermal mixing in T-junctions using URANS and Scale-resolving turbulence models in ANSYS-CFX, Nuclear Engineering and Design 240: 313-2328. http://dx.doi.org/10.1016/j.nucengdes.2009.11.008.
8. **Chapuliot, S.; Gourdin, C.; Payen, T.; Magnaud, J.P.; Monavon, A.** 2005. Hydro-thermal-mechanical analysis of thermal fatigue in a mixing tee, Nuclear Engineering and Design 235: 575–596. http://dx.doi.org/10.1016/j.nucengdes.2004.09.011.
9. **Sinkunas, S. 2009.** Effect of the temperature gradient on heat transfer and friction in laminar liquid film, Mechanika 1(75): 31-35.
10. **Pasutto, T.; Peniguel, C.; Stephan, J.M.** 2007. Effects of the upstream elbows for thermal fatigues studies of PWR T-junction using large eddy simulation, 15 International Conference on Nuclear Engineering, Nagoya, Japan.
11. **Kuczaj, A.K.; Komen, E.M.J.; Loginov, M.S.** 2010. Large-Eddy Simulation study of turbulent mixing in a T-junction, Nuclear Engineering and Design 240: 2116-2122. http://dx.doi.org/10.1016/j.nucengdes.2009.11.027
12. **Lu, T.; Jiang, P.X.; Guo, Z.J.; Zhang, Y.W.; Li, H.** 2010. Large-eddy simulations (LES) of temperature fluctuations in a mixing tee with/without a porous medium, International Journal of Heat and Mass Transfer 53: 4458-4466. http://dx.doi.org/10.1016/j.ijheatmasstransfer.2010.07.001.
13. **Launder, B. E.; Spalding, D. B.** 1972. Lectures in Mathematical Models of Turbulence, Academic Press, London, England, 169 p.
14. **Wilcox, D.C.** 1998. Turbulence Modeling for CFD, DCW Industries, Inc., La Canada, California, 460p.
15. **Menter F. R.** 1994. Two-equation Eddy-viscosity turbulence models for engineering applications, AIAA Journal 32(8):1598-1605. http://dx.doi.org/10.2514/3.12149.
16. **Launder, B.E.; Reece, G.J.; Rodi, W.** 1975. Progress in the development of a Reynolds-stress turbulence closure, J. Fluid Mech. 68(3): 537-566. http://dx.doi.org/10.1017/S0022112075001814.

M. Aounallah, M. Belkadi, L. Adjlout, O. Imine

ŠUOLIŲ MODELIAVIMAS T JUNGTYSE TURBULENTINIO IR ŠILUMOS MAIŠYMO SISTEMOSE

R e z i u m ė

Skaitmeniškai ištirtas turbulentinis ir šilumos maišymas horizontaliose T jungtyse. Šios studijos tikslas – nustatyti maišytuvo ilgį T jungtyje, kai skerspjūvyje pasiektas tolygus temperatūrinis pasiskirstymas. Nusistovėjęs trimatis turbulentinis srautas pagrindinio šalto įvado vamzdyje tiriamas esant Reinoldso skaičiui 0.7×10^5 . Tinklelis sukurtas ištęsimo būdu taip, kad stiprūs gradientai pasienio zonose būtų įvertinti kaip pridera. Keturi turbulentiškumo modeliai tęstuoti numatant nutraukti Reinoldso įtempių tenzorių galimybę: standartas *k-ε*, standartas *k-ω*, *k-ω SST* ir *RSM* modeliai. Visais modeliuotais atvejais gauti geri kokybiniai rezultatai. Kiekybiniai palyginimai rodo, kad standartiniai *k-ε* ir *RSM* modeliai įvertina sumažintas ar padidintas reikšmes, nes abu *k-ω* modeliai yra tarpusavyje artimi. Nustatyta, kad 80 colių ilgis yra pakankamas tolygiai pasiskirsčiusiai temperatūrai gauti 1°C tikslumu. Ilgesnio vamzdžio tyrimus maišymo vamzdžio ilgio įtakai nustatyti reikėtų tęsti.

M. Aounallah, M. Belkadi, L. Adjlout, O. Imine

RANS SIMULATIONS OF TURBULENT AND THERMAL MIXING IN A T-JUNCTION

S u m m a r y

The turbulent and thermal mixing in a horizontally oriented T-junction is investigated numerically. The objective of the present study is to determine the mixing length in a T-junction where homogeneous temperature distribution is established in the cross section. A steady state three-dimensional turbulent flow is considered with a Reynolds number of 0.7×10^5 at the inlet of the main cold pipe. Grid is generated in a stretched manner so that strong gradients near the wall regions are accounted for as required. Four turbulence models are tested to provide closure for the Reynolds stress tensor: the *k-ε* standard, the *k-ω* standard, the *k-ω SST* and the *RSM* models. For all simulated cases, good qualitative agreement is obtained. Quantitative comparisons show that the standard *k-ε* and the *RSM* models give too low or high predictions, whereas both *k-ω* models are reasonably close between them. It is found that a length of 80 inch is enough to get homogenous temperature if a tolerance of 1°C is considered. Further simulations on a longer pipe are strongly encouraged to assist in elucidating the length mixing determination.

Keywords: T-junction, thermal mixing, turbulence models.

Received January o6, 2012
Accepted June 03, 2013